2008 American Control Conference
Westin Seattle Hotel, Seattle, Washington, USA
June 11-13, 2008

AFM Image Based Pattern Detection for Adaptive Drift Compensation and Positioning at the Nanometer Scale

Sergey Belikov, Jian Shi, and Chanmin Su

Abstract— **The key function of AFM is to control the position of the probe according to imaging operation modes. These imaging modes yield multiple channels of data representing various probe responses to the same sample pattern. An algorithm based on the spatial and temporal correlation of the multiple channel data, corresponding to the same surface patterns, was developed to derive the pattern position with sub-pixel resolution in real time. This precise measurement of the pattern location serves as an input to an estimator of the drift velocity. An auxiliary position control was applied to compensate the drift between the probe tip and the sample. This pattern location measurement has higher noise rejection than any individual channel of the image, providing a reference location for drift compensation. Experimental data with sub nanometer drift control and nanoasperity measurements based on the auxiliary positioning are presented.**

I. Introduction

IN the last two decades atomic force microscope (AFM) has been developed well beyond the topographic imaging tool. It has become an important instrument for manipulation and material property characterizations at the nanometer scale. The precision of positioning has always been the key driver for AFM technology and scanning probe microscopy in general. In an imaging tool the uncontrolled hardware drift, such as piezo creep and thermal drift, usually causes image distortion. Many solutions based on offline correction [1], hardware optimization [2-4] and image based real-time compensation [5] were proposed.

The focus of this paper is on image-based adaptive control. Detecting an image pattern and precisely locating its coordinates enables the use an auxiliary control to compensate thermal drift. The advantage of the image-based compensation is mainly the positioning precision, which is scalable to image resolution. Close-loop scanners eliminates piezo creep but is subjected to the limitation of the sensor noise, usually in the order of a nanometer. On the other hand, image of sub angstrom lateral resolution is routinely achieved with an open loop scanner. If such atomic position or pattern positions are used as the spatial positioning references, the positioning precision is limited only by the tip resolution. Clayton and Devasia used scanning tunneling microscope image of HOPG to correct the scanner dynamics induced distortion [5]. By iterating the scanning control to reduce the positioning error they were able to achieve a few hundred Hertz scanning with much reduced distortion. The positioning error is measured by the difference between current image and a reference image. The scan size, around 1 nm, cannot be dealt with close-loop scanner or iterative feed forward control because both techniques are limited by sensor noises.

The challenge at low speed operations is drift between the SPM probe and the sample. In recent years nearly all commercial SPMs use close-loop scanner to eliminate creep induced drift and nonlinearity of the positioning actuators. However, thermal drift exists in all the systems. A well-engineered SPM system has a thermal drift rate less than a few nm/min. Such drift is not a problem for micrometer scale imaging but becomes critical limitation for nanomanipulation and measurements at nanometer scale. The pinpointed manipulation and measurements often demand long time access to the objects, such as nanotubes and quantum dots, with no drift allowed.

Several publications describe drift measurement and control systems. John et al [6] have introduced the drift measurement using cross correlation between two consecutive images and made corrections through piezo offset accordingly. The simple correction implemented is equivalent to a slow P control of position, leading to a large control error, which amounts to a few percent of the image size.

More recently Mokaber and Requicha [7] developed a drift compensation system based on Kalman filter. Although the theoretical estimation gives sub-nanometer precision for the drift compensation, the experiment exhibits more than a few nanometers control error. A close examination of the data reveals that the errors are results of cross-correlation drift measurements. In the pure prediction control, where the measurement is not involved, the positioning fluctuations are much smaller. It is obvious that a robust and precise drift measurement tool based on imaging patterns is needed in order to compensate thermal drift without causing positioning errors.

Kalman filter provides the best results when dynamics of the system is accurate and noise statistical parameters are fixed and known a priori (e.g. astronomy and navigation). Unfortunately it is not always the case for AFM where both dynamics and noise statistics may change in time and depend on sample, tip, and environment. In this situation, with inaccurate model and/or underestimated statistical parameters of the noise, Kalman filter may diverge [8], i.e. its estimation

Manuscript received September 21, 2007.

S. Belikov is with Veeco Instruments, Inc., Santa Barbara, CA 93117 USA (e-mail: sbelikov@veeco.com).
J. Shi is with Veeco Instruments, Inc., Santa Barbara, CA 93117 USA (e-mail: jshi@veeco.com).
C. Su is with Veeco Instruments, Inc., Santa Barbara, CA 93117 USA (phone: 805-967-2700; fax: 805-967-7717; e-mail: csu@ veeco.com).

has errors that are much greater than predicted by theory.

The purpose of this paper is to provide accurate and reliable tools to precisely locate the imaging pattern and implement real time control according to specific application requirements. Since AFM generates multiple image channels simultaneously, the spatial and temporal correlation of patterns in these channels can substantially enhance the robustness of the pattern detection and its position measurement. Correlations of the multi-channel data also render immunity to noises and perturbations occurred during imaging process. Furthermore the raster scanning of probe across the same pattern back and forth embeds asymmetric feedback control signatures for widely used Tapping^{TM} Mode imaging. These signatures provide a powerful tool to distinguish a true pattern from a set of noisy data. Reliable pattern positioning data enable a precise adaptive control, as demonstrated in the drift compensation, which has achieved sub-nanometer positioning accuracy over long period of time.

In this paper we also outline a framework for pattern recognition [9,10] and pattern detection taking advantage of correlation between multivariable (multi-channel) AFM images. This framework is demonstrated in practical applications of drift compensation and nanoasperity detection.

II. Patten Recognition in Multi-Channel AFM images

Apart from the primary feedback that determines tip-surface interaction, the cantilever responses generate multi-dimensional data, including height, amplitude, phase and harmonics. The forward scan (trace) and reverse scan (retrace) of the same location also provide independent information of the same pattern location. Spatial correlation of these combined data provides much better noise rejection capability, allowing surface pattern identification far beyond the bandwidth allowed by the feedback loop and system noise floor.

There are two approaches to pattern recognition and location on multi-channel images: template based and parametric based. Template based algorithms locate regions on the image that matches a known reference pattern (template). They are applicable when well defined and slowly changing patterns are available on the image. NI Vision [11] provides reliable software implementation with important algorithmic improvements. Multi-channel AFM images can improve pattern location accuracy by matching all the channels of images with their own templates, while these templates are spatially correlated.

Parametric based algorithms can be applied when interested patterns are changing from image to image and cannot be described by image template. Examples are polymeric phases undergoing transition, or slowly changing biologic samples under stimulation. These patterns, however, can be identified by a set of measurable variables such as geometrical and regression properties that are restricted to a certain parameterized region in the space of measured variables.

A parametric algorithm based on geometrical patterns and spatial correlation of the combined images was developed to locate the surface pattern with sub-pixel resolution in real time.

The parametric patterns in the multi-channel images are identified by a set of *thresholds* τ_i, (i=1,..,n_τ), one for each channel (with the trace and retrace data considered as different channels). These thresholds divide the pixels on every related image channel into two regions (with pixel values below and above the thresholds) and define the *particles* on the images, i.e. connected regions of pixels with values above the thresholds. The coordinates of the pixel with predefined location (e.g. location of the peak value inside the particle or a well defined corner of the particle) are called a *location of the particle*. Particles appear in different imaging channels are called *related particles* if they satisfy certain conditions (including closeness of their locations).

The particle analysis is implemented firstly for nanoasperity (NA) detections. Nanoasperities are small protrusions with the height ranging from sub-nanometer to a few nanometers and lateral dimension of 10 to 20 nm. The quality control of data storage industry demands detection of such features in a raster scanning size of 20 µm, where the feature height is in the same magnitude of the noise floor. Figure 1 shows an example of the AFM data. The streak shaped short lines in the height images are due to either occurrence of the nanoasperity event or system noise, including mechanical perturbations. Only 6 of the events are qualified nanoasperities. On the other hand, none of the single image data can generate the information without ambiguity. Multi-channel particle analysis will help to qualify the true events in this case.

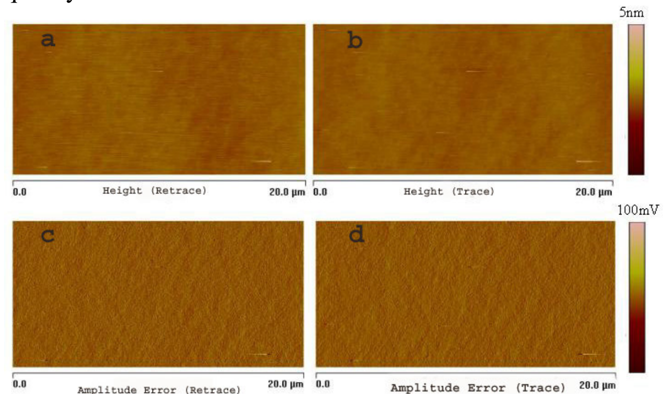

Figure 1. Tapping mode^{TM} image of a data storage media with a-d represent height and amplitude images.

Nanoasperity detection problem with its specific constraints on the particle's parameters utilizes the parametric based algorithms. Besides multi-channel geometrical measurements this problem uses regression characteristics of trace and retrace images.

III. Adaptive Control of Drift Compensation

Pattern recognition provides a measurement of the position of the pattern. A controller is needed to properly compensate the position changes. Drift compensation relies on drift measurements based on pattern recognition. In practice,

depending on application, one can use either specialized pattern location methods or well developed general technique based on locating regions on the image that matches a known reference template. Without loss of generality we can assume that reference position of the pattern is (x_1=0, x_2=0), where ($x_1(t)$, $x_2(t)$) is the drifting location of the pattern (horizontal and vertical).With this notation, a simple dynamics of velocity controlled drift compensation system is:

$$\dot{x}_i(t) = u_i(t) + v_i^d(t), \quad i = 1,2 \tag{1}$$

where $u_i(t)$ is the controlled velocity, and v_i^d is velocity of the drift. In this model we assume that the drift velocity is slow varying in most of the time and can be considered as a constant parameter of simple dynamic model (1). Abrupt change of condition rarely occurs due to large thermal inertia of the AFM systems. The position of the pattern can be measured directly, e.g. by image pattern recognition:

$$(\hat{x}_1(t), \hat{x}_2(t)) = \text{PatRec(Image)} = (x_1(t), x_2(t)) + \text{error}$$

where ^ denote estimated (or measured) number in contrast to actual physical value. PatRec(Image) is a notation of any image location measurement based on pattern recognition outlined in Section II.

A proposed adaptive control algorithm is based on simple adaptation of the Friedland's parameter estimator [12]. According to separation principle controller design and state/parameter estimator can be designed separately. Controller design assumes that all states and parameters are known and controller implementation uses the outputs from the estimator as values of the unknown states and parameters.

The adaptive approach was chosen as alternative to systematic methods such as LQG (Kalman Filter coupled with Linear Quadratic Regulator) or H∝ because a justifiable design model for drift in AFM cannot be developed and the best a priori knowledge of the drift cannot provide more than simple 1st order model (1). With significant deviations from the model and varying environmental conditions Kalman filter may diverge and provide estimation error significantly larger than theoretical calculations. In such conditions the adaptive control described in this section performs better and exhibits higher stability.

A. Controller Design

In the proposed controller the compensation velocity is calculated by a simple model inversion formula

$$u_i = -\hat{v}_i^d - \lambda_i x_i, \quad i = 1,2 \tag{2}$$

The first term on the right side of (2) is the open-loop drift speed compensator and the second is the gain for position offset to make the control system (1) asymptotically stable (remind that x_i=0 is the reference position). With this control the dynamics of (1) becomes

$$\dot{x}_i = -\lambda_i x_i, \quad i = 1,2 \tag{1'}$$

and is asymptotically stable.

B. Drift Velocity Estimator Design

The following estimator for the drift velocity (simple Friedland's estimator [12]) is used:

$$\begin{aligned} \hat{v}_i^d &= \alpha_i x_i + z_i, \quad i = 1,2 \\ \dot{z}_i &= -\alpha_i \left(\hat{v}_i^d + u_i\right) \end{aligned} \tag{3}$$

where α_i is a gain of the estimator (see below).

Assuming that drift acceleration is significantly slower than controller dynamics, it is important to verify the property of the estimator that estimation $\hat{v}_i^d$ approaches the correct constant value v_i^d . To do this let us introduce the error of estimation

$$e_i(t) = v_i^d - \hat{v}_i^d(t)$$

With unknown constant (or slow varying) v_i^d , the dynamics of the error can be derived following (1) and (3):

$$\dot{e}_i = -\alpha_i e_i, \quad i = 1,2$$

The error converges to zero with ascending time.

C. Integration of Observer

The equations in (1), (2) and (3) for i=1 and i=2 are independent and in further presentation the subscript i will be omitted for simplicity.

Measurements of $x(t)$ are taken at discrete moments. Assume that previous measurement was taken at t=0 and current measurement at $t=\tau$, and the values of x are $x(0)$ and $x(\tau)$. Applying constant control between the measurements (calculated by (2) with $x=x(0)$) and assuming constant unknown drift velocity, the solution of (1) and (2) is

$$x(t) = x(0) + \frac{x(\tau) - x(0)}{\tau} t, \quad 0 \le t \le \tau$$

Combining this $x(t)$, equation (3) can be written as

$$\dot{z} = -\alpha z + at + b$$

where

$$a = -\alpha^2 \frac{x(\tau) - x(0)}{\tau}$$
$$b = -\alpha^2 x(0) - \alpha u(0)$$

and its solution becomes

$$z(\tau) = \frac{a}{\alpha}\tau - \left(\frac{a}{\alpha^2} - \frac{b}{\alpha}\right) + \left[z(0) + \left(\frac{a}{\alpha^2} - \frac{b}{\alpha}\right)\right] e^{-\alpha\tau} \tag{4}$$

D. Drift Compensation Algorithm

Based on formulas (2), (3) and (4) the following drift compensation algorithm is proposed.

0. Initialization:

$$\mathbf{x}_{\mathbf{old}} = 0; \quad \mathbf{z}_{\mathbf{old}} = 0; \quad \mathbf{u}_{\mathbf{old}} = 0 \quad \Rightarrow \hat{\mathbf{v}}^{\mathbf{d}}_{\mathbf{old}} = 0$$

Iterate in the loop:

1. Measure new drift $\mathbf{x}_{\mathbf{new}}$ and time Δt between the latest two measurements (using PatReq(Image))

2. Calculate

$$\mathbf{z}_{\mathbf{new}} = \frac{\mathbf{a}}{\boldsymbol{\alpha}}\Delta t - \left(\frac{\mathbf{a}}{\boldsymbol{\alpha}^2} - \frac{\mathbf{b}}{\boldsymbol{\alpha}}\right) + \left[\mathbf{z}_{\mathbf{old}} + \left(\frac{\mathbf{a}}{\boldsymbol{\alpha}^2} - \frac{\mathbf{b}}{\boldsymbol{\alpha}}\right)\right] e^{-\boldsymbol{\alpha}\Delta t}$$

where

$$\mathbf{a} = -\boldsymbol{\alpha}^2 \frac{\mathbf{x}_{\text{new}} - \mathbf{x}_{\text{old}}}{\Delta t}; \quad \mathbf{b} = -\boldsymbol{\alpha}^2 \mathbf{x}_{\text{old}} - \boldsymbol{\alpha}\mathbf{u}_{\text{old}}$$

3. Calculate new drift velosity estimate

$$\hat{\mathbf{v}}_{\text{new}} = \boldsymbol{\alpha}\mathbf{x}_{\text{new}} + \mathbf{z}_{\text{new}}$$

4. Calculate new control

$$\mathbf{u}_{\text{new}} = -\hat{\mathbf{v}}^{d}_{new} - \boldsymbol{\lambda}\mathbf{x}_{\text{new}}$$

and apply it to the system.

5. Redefine

$$\mathbf{x}_{\text{old}} = \mathbf{x}_{\text{new}}; \quad \mathbf{z}_{\text{old}} = \mathbf{z}_{\text{new}};$$

$$\mathbf{u}_{\text{old}} = \mathbf{u}_{\text{new}}; \quad \hat{\mathbf{v}}^{\mathbf{d}}_{\text{old}} = \hat{\mathbf{v}}^{\mathbf{d}}_{\text{new}}$$

6. go to step 1.

End of the loop

The adjustable gains $\boldsymbol{\lambda}$ and $\boldsymbol{\alpha}$ are absolute values of negative eigenvalues of the system under control (1'), -$\boldsymbol{\lambda}$, and the dynamics of estimator's error, -$\boldsymbol{\alpha}$. Without discretization both dynamics are stable.

With discretization, however, stability of the system may be lost. With control $\mathbf{u}$ constant between the measurements, the position $\mathbf{x}$ is drifting linearly in t according to equation (1). The linear term of the solution of equation (1') is

$$\mathbf{x}(\Delta t) = \mathbf{x}(0)[1 - \lambda\Delta t]$$

To avoid oscillation around zero (at least in the model), the following condition should hold: $\boldsymbol{\lambda}<(\Delta t)^{-1}$, or in practice,

$$\lambda = \frac{k}{\Delta t}. \quad k \in [0.05, 0.8]$$

There are no specific theoretical constrains on $\boldsymbol{\alpha}$. The estimator of drift velocity $\hat{v}_i^d$ in (3) is implemented using two latest measurements; and continuous model (4) for the estimator's state z_i is implemented between the measurements. In practice, to be tolerant to noise,

$$\alpha = k\lambda, \quad k \in [3, 10]$$

These gains should be chosen interactively based on operation condition. Gain scheduling is useful to quickly achieve rough convergence with higher gains and then make the gains smaller to adapt to the noise.

A simplified block diagram of the system is shown in Figure 2. Imaging hardware (AFM) outputs images with drifted patterns. The Image Processing (Pattern recognition) block implements step 1 of the algorithm, i.e. measures the drift by any method of pattern recognition outlined above. Drift velocity estimator implements steps 2 and 3, and the Compensator implements step 4. Control velocity can be commanded by DSP hardware that applies smooth change of offset at high update rate, up to 100 kHz for the existing AFM controller. If this hardware option is not available or justifiable, AFM image offsets can also be applied automatically between the scan lines or frames by adding $\mathbf{u}\Delta t$ to the current offset, where Δt is a predicted time between the previous and the next measurements. This time can be accurately estimated based on AFM sample rate. Scheduler changes gains of Compensator and Estimator and update pattern when necessary. Updating pattern for drift compensation application may mean updating a template; alternatively, for parametric pattern recognition, it means updating parameters of the evolving pattern.

IV. Experimental Results

The drift control characteristics were performed using a Veeco Multimode™ AFM in an open lab environment. Temperature change was not controlled but monitored, with a change of 2°C throughout a typical cycle of 24 hours. The nanoasperity experiments were using a Dimension™ 3100 since the measurements involve large sample and automatic sample site exchange.

A. *Drift Control*

The pattern recognition algorithm discussed in the previous sections measures the tip position relative to the sample. An example is shown in figure 3. Part of the characteristic pattern in figure 3a is selected as the anchor pattern, where 4 to 6 data channels corresponding to the pattern spatial and temporal relations were simultaneously acquired. The patterns are

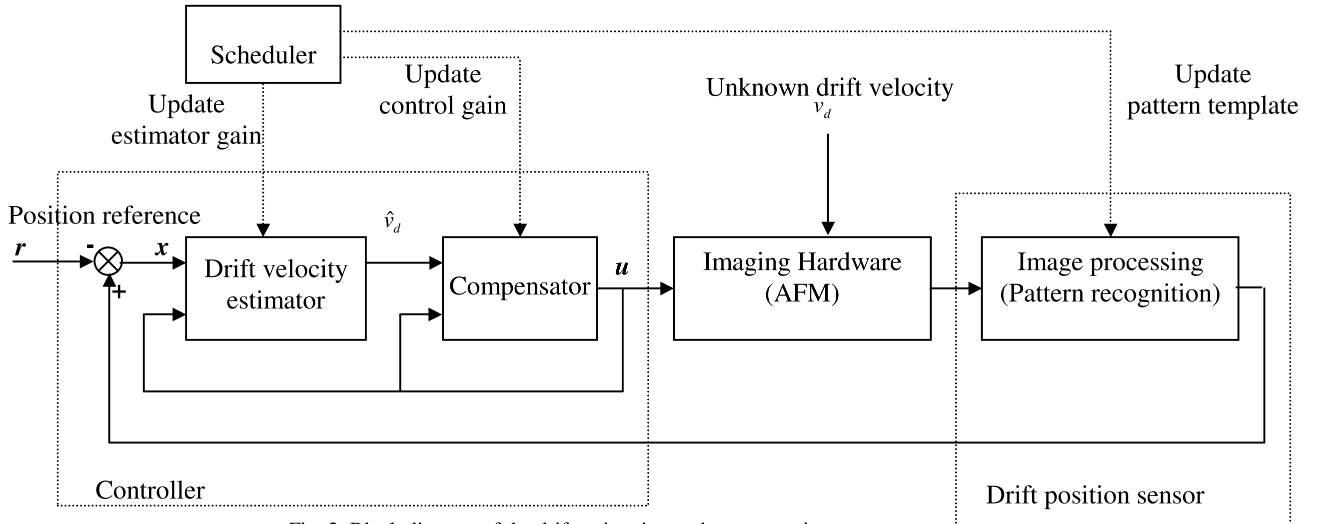

Fig. 2. Block diagram of the drift estimation and compensation

compared with templates, created through the initial image showing in figure 3a. Selection of a template should contain sharp edge in both x and y directions. The spatial and temporal correlations between the templates were used to determine the position of the pattern. The translation of the pattern is recorded as the measurement of the drift. As a result of the real time drift compensation the pattern drift is within a nanometer in the 12-hour period (figure 3b).

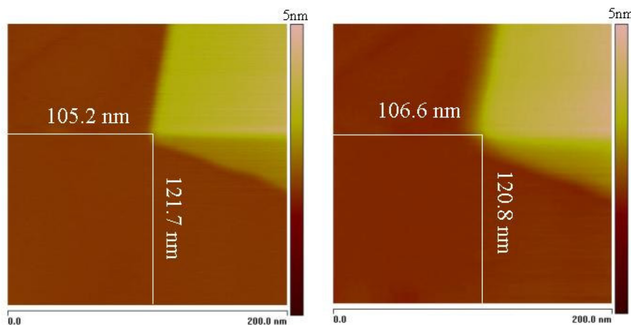

Figure 3. Image of HOPG at a joint of triple atomic facets. (a). Left: The pattern used to monitor the drift at the control start.; (b). right: the same pattern after 12 hours. The distances in the images represent the position of the anchor point throughout the controlling period.

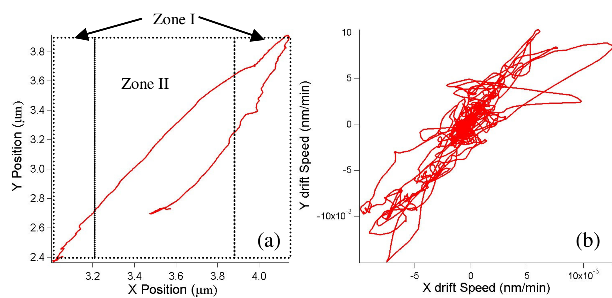

Figure 4. (a). Trajectory of the tip apex relative to the sample monitored in an over night cycle and (b) trajectory of the drift velocity vector.

The control actions to maintain the anchoring position reflect the drift of the system. A typical drift monitored by the estimator is shown in figure 4 for a 24 hours period. In figure 4a there are two types of drift corresponding to zone I and II. The main difference of these two periods relates to air convection flow when the central air conditioning system is turned on and off (zone I and II). As the convection flow equilibrating the system enters zone II. In zone II the drift trajectory is predictable in a relatively long period of time and the feedback can rely mainly on the value of the drift velocity predicted by the estimator. In this case the measurement of tip location can be interrupted for manipulation and point-and-shoot measurements. In zone I where the convection flow perturbs the drift behavior the observer (estimator) can only make short-term prediction, the position measurement must stay active meaning the imaging of the anchor pattern should proceed. The temperature change in the period is 2.3 ^{o}C. However the smoothness of the trajectory is unrelated to the temperature variation.

The trajectory of the drift velocity vector over the same period is shown in figure 4b. While the most data are concentrated at the center, there are traces far off the center, amount to tens of nm drift. The randomness of these relative high-speed drifts re-emphasized the need of the iterative model updating.

The detailed results of the drift control are shown in figure 5. In figure 5a, curve 1 represents the controller action u_x in equation (4); curve 2 is the drift velocity in x direction from the estimator $\widehat{v}_x^d$. The initial state of the controller and estimator are zeros due to lack of knowledge of the drift. As the measurements builds up the drift rate is determined more accurately, the controller ramps up the control until the drift is compensated. The actual positioning error is shown in fig. 5b. The horizontal curve represents a zero drift target, as the control reference. The controller reaches nanometer precision in about half an hour. Since the observer has now a fully established steady drift model the control loop gain will be dominated by the predicted drift until the measurement indicated a larger error. The model will keep updating control gradually according to the new measurement. The long-term stability is shown in figure 5c. The data reflect the actual tip position relative to the anchor pattern. As can be seen the positioning error is within 1 nm from the target over an extended time. Y-axis control has the same characteristics and noise level.

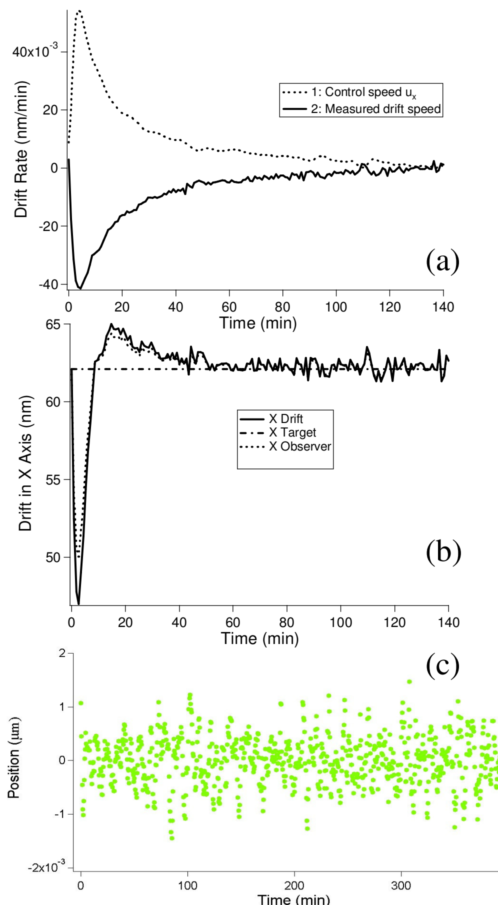

Figure 5. The drift control results. (a). curve 1. The control speed u_x; curve 2. The measured drift speed. (b). Position measurement as a function of time.

Dash-dotted line: reference position; solid line: measured position; dotted line: observer output. (c).long term stability with position as a function of time.

It is worth to mention that the above controls are performed for an open loop scanner in which the drift also included piezo hysteresis. Since our sensing element is the tip itself, the correction will compensate any drift regardless its physical origin.

B. Nanoasperity Detection and Measurements

Figure 6 illustrates AFM images of a typical nanoasperity. Figure 6a is a 10 Hz scanning data with the pixel resolution of 2nm/pixel. The shape of the nanoasperity and the surface roughness is accurately measured. In the conventional application a scanning of 20μm area is needed to increase inspection coverage. However, even at 0.5 Hz scan rate the bandwidth of the feedback is still insufficient to track the small particles within a few pixels. The data zoom shown in figure 6b only gives an indication of the nanoasperity event but not nearly the quality of the data for the geometric measurement. Figure 6c is the same 20 um scan but with 7 times higher speed. One can see the nanoasperity event is displayed in the survey data with further deteriorated quality. Since the nanoasperity event is already clearly determined, the higher speed scan offers the advantage to reduce the site survey from nearly an hour to minutes. Using the scheme of combining survey scan of figure 6c and detail scan of figure 6a not only the site (20X10 μm) survey time can be reduced but the data qualify can be substantially improved.

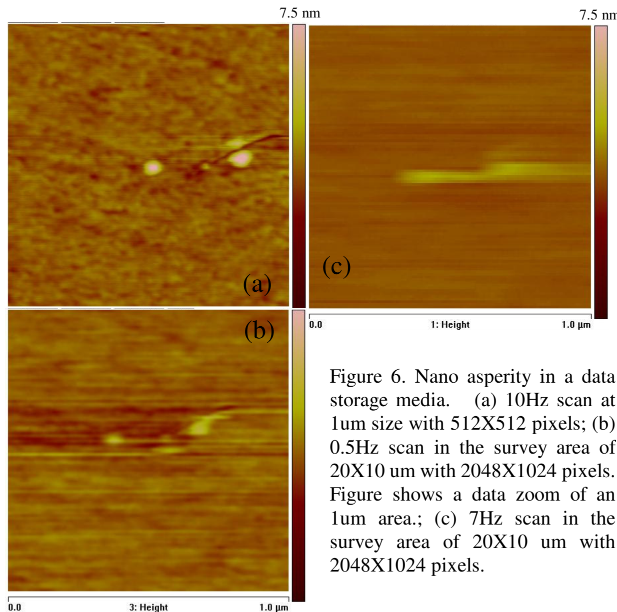

Figure 6. Nano asperity in a data storage media. (a) 10Hz scan at 1um size with 512X512 pixels; (b) 0.5Hz scan in the survey area of 20X10 um with 2048X1024 pixels. Figure shows a data zoom of an 1um area.; (c) 7Hz scan in the survey area of 20X10 um with 2048X1024 pixels.

The challenge is to detect the nanoasperity without fault within the data with low signal to noise ratio. These nanoasperities are not even visible to operator examination of the image. The noise level in all the images is comparable to the pattern. None of these individual images can provide a well-defined parameter space to locate the patterns. However, multi-channel particle analysis outlined in section II gives positive identification of nanoasperties even when their heights are in the noise level.

In the nanoasperity application the parametric pattern detection is critical and a multi-channel measured variables have to be used to minimize the missing and false hits. After accurately locating nanoasperity the controller simply offsets the tip to the point of interest automatically and performs a high quality measurement.

The parametric pattern measurement from multiple channels simultaneously provides a robust mechanism in catching nanoasperities.

V. Summary

A pattern detection algorithms based on multi-channel data analysis in real time have been developed and used in control applications. The detection of the patterns and precisely locating their positions allow the measurements and compensation of the system drift or zoom-in scan for high quality data. A digital controller with a positioning precision of 1 nm compensates the drift over long period of time in an uncontrolled open environment.

Acknowledgment

This work is supported by NIST Advanced Technology Program with the contract number 70NANB4H3055.

REFERENCES

[1] V. Yu. Yurov and A. N. Klimov, " Scanning tunneling microscope calibration and reconstruction of real image: Drift and slope elimination," Rev. Sci. Instrum., vol 65 (5), May 1994.

[2] A. Beyder, C. Spagnoli, and F. Sachs, “Reducing probe dependent drift in atomic force microscope with symmetrically supported torsion levers,” Rev. Sci. Instrum., vol 77 (5), May 2006.

[3] S. M. Altmann, P.-F. Lenne, J.-K. and H. Hörber, “Multiple sensor stabilization system for local probe microscopes,” Rev. Sci. Instrum., vol 72 (1), January 200, pp. 142–149.

[4] H. J. Hug, Th. Yung, and H.-J. Göntherodt, “A high stability and low drift atomic force microscope,” Rev. Sci. Instrum., vol 63 (8), 1992, pp. 3900–3904.

[5] G. M. Clayton and S. Devasia, "Image-based compensation of dynamic effects in scanning tunnelling microscopes", *Nanotechnology*, vol 16, , 2005, pp 809–818

[6] S. John T. van Noort, Kees O. van der Werf, Bart G. de Grooth, and Jan Greve, " High Speed Atomic Force Microscopy of Biomolecules by Image Tracking", Biophysical Journal, vol 77, October 1999, pp 2295–2303.

[7] B. Mokaberi, A. Requicha, “Drift compensation for automatic nanomanipulation with scanning probe microscopes”, IEEE Trans. On Auotomation Sci. and Eng., vol. 3 (3), July 2006, pp. 199–207.

[8] F. Schlee, et al, Divergence in Kalman Filter, in *Kalman Filtering: Theory and Applications*, H. Sorenson, Ed., New York: IEEE Press, 1985, pp. 144–150.

[9] R. Duda, P. Hart, D. Stork, *Pattern Classification*. New York: Wiley & Sons, 2001.

[10] Gonzalez, Wood, *Digital Image Processing*. Upper Saddle River, NJ: Prentice Hall, 2008, ch. 12.

[11] *NI Vision Concept Manual*. Austin, TX, National Instruments, 2007, ch. 12.

[12] B. Friedland, *Advanced Control System Design*, Englewood Cliffs, NJ: Prentice Hall, 1996, pp. 318-324.